Journal of the American Statistical Association

ISSN: (Print) (Online) Journal homepage: https://www.tandfonline.com/loi/uasa20

A Mechanistic Model of Annual Sulfate Concentrations in the United States

Nathan B. Wikle, Ephraim M. Hanks, Lucas R. F. Henneman & Corwin M. Zigler

To cite this article: Nathan B. Wikle, Ephraim M. Hanks, Lucas R. F. Henneman & Corwin M. Zigler (2022): A Mechanistic Model of Annual Sulfate Concentrations in the United States, Journal of the American Statistical Association, DOI: 10.1080/01621459.2022.2027774

To link to this article: https://doi.org/10.1080/01621459.2022.2027774

JOURNAL OF THE AMERICAN STATISTICAL ASSOCIATION
2021, VOL. 00, NO. 0, 1–12: Applications and Case Studies
https://doi.org/10.1080/01621459.2022.2027774

A Mechanistic Model of Annual Sulfate Concentrations in the United States

Nathan B. Wikle[a], Ephraim M. Hanks[b], Lucas R. F. Henneman[c], and Corwin M. Zigler[a]

[a]Department of Statistics and Data Sciences, University of Texas at Austin, Austin, TX; [b]Department of Statistics, Pennsylvania State University, University Park, PA; [c]Department of Civil, Environmental, and Infrastructure Engineering, George Mason University, Fairfax, VA

ABSTRACT

Understanding how individual pollution sources contribute to ambient sulfate pollution is critical for assessing past and future air quality regulations. Since attribution to specific sources is typically not encoded in spatial air pollution data, we develop a mechanistic model which we use to estimate, with uncertainty, the contribution of ambient sulfate concentrations attributable specifically to sulfur dioxide (SO_2) emissions from individual coal-fired power plants in the central United States. We propose a multivariate Ornstein–Uhlenbeck (OU) process approximation to the dynamics of the underlying space-time chemical transport process, and its distributional properties are leveraged to specify novel probability models for spatial data that are viewed as either a snapshot or time-averaged observation of the OU process. Using US EPA SO_2 emissions data from 193 power plants and state-of-the-art estimates of ground-level annual mean sulfate concentrations, we estimate that in 2011—a time of active power plant regulatory action—existing flue-gas desulfurization (FGD) technologies at 66 power plants reduced population-weighted exposure to ambient sulfate by 1.97 $\mu g/m^3$ (95% CI: 1.80–2.15). Furthermore, we anticipate future regulatory benefits by estimating that installing FGD technologies at the five largest SO_2-emitting facilities would reduce human exposure to ambient sulfate by an additional 0.45 $\mu g/m^3$ (95% CI: 0.33–0.54). Supplementary materials for this article are available online.

ARTICLE HISTORY
Received October 2020
Accepted December 2021

KEYWORDS
Air pollution; Ornstein-Uhlenbeck process; SDEs; Space-time processes; Spatial statistics

1. Introduction

Sulfur dioxide (SO_2) emissions from coal-fired power plants are a major source of anthropogenic air pollution (Rowe 1980). Upon release into the atmosphere, SO_2 compounds are simultaneously acted upon by chemical and physical processes, forming particulate sulfates (SO_4^{2-}) which are then transported across space. Exposure to sulfate aerosols is associated with many adverse human health outcomes, including decreased lung function (Ng et al. 2019), increased risk of cardiovascular disease (Bai et al. 2019b), and lung cancer (Bai et al. 2019a). Sulfate also represents one component of fine particulate matter (PM2.5), regulations for which comprise the most beneficial—and costly—federal regulations in the United States (Dominici, Greenstone, and Sunstein 2014). In addition, sulfur dioxide emissions contribute to acidic deposition (U.S. EPA 2003), and have been linked to negative radiative forcing, resulting in short-lived cooling of the climate (Ward 2009; Kaufmann et al. 2011; Aas et al. 2019). Consequently, assessing the regulatory impacts of various SO_2 emissions scenarios on ambient SO_4^{2-} concentrations may lead to an improved understanding of regional environmental and public health outcomes.

Importantly, the dependence of air pollution concentrations on upwind emissions sources suggests that known atmospheric pollution transport dynamics should be included in the analysis of spatial air pollution data. The inclusion of process dynamics is especially important when inferring the effect of power plant emissions on observed public health outcomes across a large spatial domain (Zigler, Forastiere, and Mealli 2020; Zigler and Papadogeorgou 2021). Existing atmospheric pollution analyses often fall into two camps: numerical models, such as chemical transport models (Stein et al. 2015), plume models, and their so-called reduced-form hybrids (Foley et al. 2014; Heo, Adams, and Gao 2016), in which process dynamics are used to simulate many individual-level trajectories of point-source pollutants, and phenomenological statistical models which seek to accurately interpolate regional air pollution concentrations from a variety of monitoring systems (van Donkelaar et al. 2019; Guan et al. 2020). Although these models have proved useful, their utility is limited by the lack of data-driven inference in the numerical models, and the lack of incorporation of known mechanistic processes in the statistical models, respectively.

In this paper, we seek to develop a statistical model of yearly-aggregated SO_4^{2-} concentrations attributed to coal-fired power plant SO_2 emissions, in which the known physical processes governing pollution transport directly inform the first and second-order structure of our statistical model. The advantages of this modeling approach include its ability to infer process dynamics and stochastic fluctuations on a time-scale of interest and to provide reasonable forecasts of future air pollution levels from spatial data alone. In doing so, we construct a new class of *mechanistic spatial models* which allows us to model spatial SO_4^{2-} measurements based on a dynamic physical model appropriate for this system.

CONTACT Nathan B. Wikle nbwikle@utexas.edu Department of Statistics and Data Sciences, The University of Texas at Austin, Austin, TX.
Supplementary materials for this article are available online. Please go to www.tandfonline.com/r/JASA.

In particular, we construct a general class of mechanistic spatial models from the multivariate Ornstein-Uhlenbeck (OU) process. These mechanistic models can accommodate spatial data viewed as either a transient or stationary "snapshot" of a spatio-temporal process, or as a time-averaged observation of a space-time process over a finite time interval. Many common spatial data can be seen as a special case of one of these scenarios. The models we develop are flexible enough to handle many linear dynamical systems, and space-time noise is explicitly included in the OU process construction. Importantly, both the process dynamics and temporal window of observation dictate the mean and spatial covariance structure of the model; in special cases, these resemble familiar specifications of spatial autocorrelation. These methods are well-suited for our analysis of the impact of coal-fired power plant sulfur dioxide emissions on average atmospheric sulfate concentrations across the central United States; the mechanistic spatial model allows for probabilistic forecasts of average SO_4^{2-} concentrations under alternative emissions scenarios that are unavailable when using traditional phenomenological models. Such statistical forecasting with complete uncertainty quantification promises to advance current methodology for environmental risk assessment that relies on deterministic physical–chemical models to predict pollution under various counterfactual scenarios.

The remainder of the article is organized as follows. In Section 2, we provide an overview of the particulate sulfate data and its connection to coal-fired power plant emissions. We then present a dynamic physical model of atmospheric sulfate concentration as a motivating space-time process from which spatial data are observed. In Section 3, we construct a general framework for analyzing spatial data from a broad class of space-time processes, emphasizing how process dynamics and the type of spatial observation can be leveraged to specify mechanistic models for spatial data. In Section 4, we analyze the 2011 average sulfate pollution in the central United States attributed to sulfur dioxide emissions from power plants. Finally, in Section 5 we discuss possible extensions to our mechanistic approach for modeling spatial air pollution data.

2. Atmospheric Sulfate and Coal-Fired Power Plants

Given the known association between exposure to fine particulate matter (including sulfate) and a number of chronic diseases (Brook et al. 2010), the United States has implemented federal regulations to limit emissions from sources of anthropogenic air pollution (Dominici, Greenstone, and Sunstein 2014). Consequently, estimating the effect of such regulation on regional public health outcomes is a major effort in environmental epidemiology. Air pollution concentrations may be heavily dependent on upwind emissions sources, and it is often critical that the (nonstationary) dependence between pollution sources and concentrations be accounted for in such an analysis. For example, when estimating the causal effect of coal-fired power plant emissions reductions on Medicare hospitalization rates across the United States, Zigler, Forastiere, and Mealli (2020) use a chemical transport model to define a spatial interference network, mapping population centers to the upwind emissions facilities of greatest impact. In other words, the emissions from a single power plant propagate across space, impacting health outcomes across a large spatial extent. Without accounting for this complex dependence structure, statistical inference on the environmental and public health impacts of power plant emissions is limited.

With this spatial interference in mind, we analyzed average 2011 sulfate concentrations across the central United States (Figure 1). Estimated annual average sulfate concentrations ($\mu g/m^3$) were obtained from the Dalhousie University Atmospheric Composition Analysis Group, version V4.NA.02 (van Donkelaar et al. 2019). These data were supplemented with annual coal-fired power plant SO_2 emissions totals from the U.S. EPA's Air Markets Program Database (AMPD) (U.S. EPA 2016; Henneman et al. 2019), as well as with meteorological data (e.g., average wind velocity, precipitation, etc.) from the NCEP/NCAR reanalysis database (Kalnay et al. 1996). In our analysis, we assess the influence of annual sulfur dioxide emissions totals (Figure 1(a)) and average wind velocity (Figure 1(b)) on 2011 sulfate levels. We propose a mechanistic modeling approach to account for the potentially large spatial footprint of upwind emissions sources. In addition, we provide probabilistic forecasts of SO_4^{2-} concentrations under alternative emissions scenarios, and identify the regulatory policy which is expected to best reduce human exposure to atmospheric SO_4^{2-}. In order to construct a mechanistic model for spatial air pollution data, we first present a physical model of the space-time emissions process.

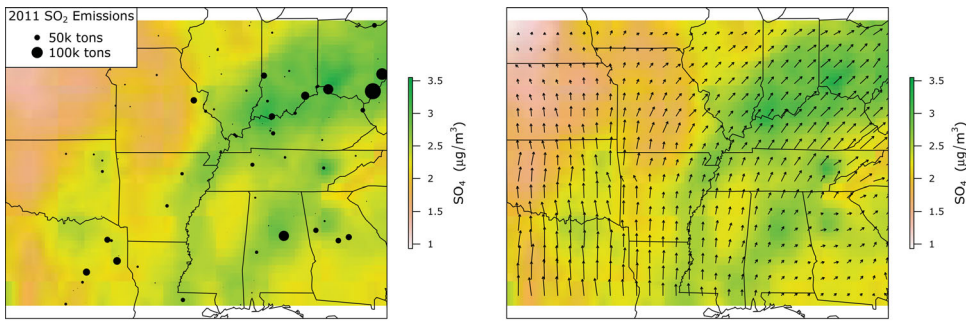

(a) SO_2 emissions sources

(b) Average yearly wind velocities (10 m)

Figure 1. Average 2011 sulfate concentrations ($\mu g/m^3$) across the central United States, including (a) coal-fired power plant locations, with point size weighted by total 2011 SO_2 emissions (in tons), and (b) the 2011 average wind velocities (height = 10 m).

2.1. A Physical Model of Sulfate Concentration

The physical dynamics governing sulfate aerosols can be approximated with a mechanistic representation of atmospheric chemical transport. The development of realistic chemical transport models is a broad and active area of research in atmospheric chemistry (see, e.g., Seinfeld and Pandis (2016) for details). However, for the purposes of this analysis, we consider a relatively simple physical model of sulfate transport that necessarily sacrifices complexity for increased spatial and temporal scalability, paralleling recent trends in atmospheric modeling using so-called reduced-complexity models (Tessum, Hill, and Marshall 2017). The model characterizes changes in aerosol concentration as a result of four key processes: advection-diffusion, atmospheric deposition (dry and wet), chemical reaction, and emission. These processes can be specified with a differential equation augmented by a mean-zero noise process; the addition of uncertainty results in a stochastic partial differential equation (SPDE).

Let $y_i(t) \equiv y(\boldsymbol{s}_i, t)$ denote the atmospheric SO_4^{2-} concentration at location $\boldsymbol{s}_i \in \mathcal{D}$ and time t, where $\mathcal{D} \subset \mathbb{R}^2$ is the continuous spatial domain of interest. We assume that the physical process can be written as

$$dy_i(t) = \left[(\gamma\Delta + \alpha\, \boldsymbol{v}_i \cdot \nabla - \delta)\, y_i(t) + \eta z_i(t)\right] dt + \xi(\boldsymbol{s}, t), \quad (1)$$

where $\gamma\Delta$ denotes homogeneous spatial diffusion with rate γ (note, $\Delta \equiv \frac{\partial^2}{\partial x_1^2} + \frac{\partial^2}{\partial x_2^2}$); advection due to wind is defined by the advective derivative $\boldsymbol{v}_i \cdot \nabla \equiv v_{x_1}\frac{\partial}{\partial x_1} + v_{x_2}\frac{\partial}{\partial x_2}$, where $\boldsymbol{v}_i = (v_{x_1}, v_{x_2})'$ is the velocity vector at location $\boldsymbol{s}_i$; deposition occurs at rate δ; and $\eta z_i(t)$ indicates the addition of SO_4^{2-} due to the reaction of the local concentration of SO_2, which we denote as $z_i(t)$. Finally, $\xi(\boldsymbol{s}, t)$ denotes Gaussian noise, which represents space-time varying sources and sinks of SO_4^{2-} that are otherwise unaccounted for in the model, such as fluctuations caused by shifting weather patterns, landscape variability, sulfate emissions from motor vehicles, etc.

The predominant source of atmospheric SO_4^{2-}—and the source of SO_4^{2-} that we are most interested in analyzing—is thought to be sulfur dioxide (SO_2) emissions from coal-fired power plants (Massetti et al. 2017). Therefore, we assume that SO_4^{2-} is introduced to the system through a reaction term which depends on the local concentration of SO_2 attributed to coal-fired power plant emissions. In addition, for computational convenience we assume that the advection-diffusion process for SO_2 is the same as for SO_4^{2-}. Thus, letting $z_i(t)$ denote the local SO_2 concentration, and βX_i the rate of SO_2 emission from a coal-fired power plant located at $\boldsymbol{s}_i$, with an annual emissions total of X_i, the physical model of SO_2 concentration is

$$dz_i(t) = \left[(\gamma\Delta + \alpha\boldsymbol{v}_i \cdot \nabla - \eta)\, z_i(t) + \beta X_i\right] dt. \quad (2)$$

Together, Equations (1) and (2) define a physical model linking SO_2 emissions from coal-fired power plants to atmospheric SO_4^{2-} concentrations. The equations define a reaction-diffusion system, with randomness introduced via the noise process in Equation (1). Notably, the velocity vector $\boldsymbol{v}_i$ is assumed to be constant in time throughout the coupled system; it is the average 2011 wind velocity vector at location $\boldsymbol{s}_i$ (Figure 1(b)). Although wind velocities exhibit some temporal variability (see Section 3 in the supplementary materials for a comparison with 2011 monthly wind velocities), our analysis ultimately focuses on annually-averaged sulfate concentrations attributed to annual SO_2 emissions, and the assumption of constant wind allows us to derive a computationally efficient statistical distribution for the annual average sulfate concentration. We discuss possible extensions to a model with time-varying velocity in Section 5.

3. Constructing Spatial Models from Ornstein–Uhlenbeck Processes

3.1. Mechanistic Statistical Models for Spatial Data

The physical dynamics defined in Section 2.1 serve as a scaffolding from which we build a statistical model for the annual sulfate data. Importantly, the observed sulfate data are spatially referenced, and we seek to define a joint probability distribution in which the physical dynamics inform the first and second-order structure of the model. The construction of such *mechanistic* models for spatial data may be beneficial to the study of a variety of scientific systems, as most spatial data can be similarly understood as arising from a spatio-temporal generating process.

When spatial observations are made repeatedly in time, science-based dynamic spatio-temporal models have been used to great effect (Wikle and Hooten 2010; Cressie and Wikle 2011), often enabling more accurate probabilistic forecasts and scientific insights than traditional descriptive models (Hefley et al. 2017). In contrast, statistical models for explicitly spatial data—that is, spatially referenced data without temporal replication—are often chosen without consideration of the underlying dynamic process. Instead, spatial statistical models are mostly phenomenological, focused on modeling (a) the correlation between the process mean and (local) covariates, and (b) residual autocorrelation through the addition of a spatial random effect (Banerjee, Carlin, and Gelfand 2004). The random effect is often chosen to have a Gaussian process (GP) prior distribution, where the GP covariance is dictated by the spatial support of the data. Common choices include the Matérn class of covariance functions for point-referenced spatial data (cf. Cressie 1993), and conditional autoregressive (CAR) or simultaneous autoregressive (SAR) covariance structures for areal/lattice data (Besag 1974; Cressie 1993; Ver Hoef, Hanks, and Hooten 2018). Although some classes of GP covariance functions have links to differential equations (see, e.g., Whittle 1954, 1962 and Lindgren, Rue, and Lindström 2011), in practice the predominant consideration when choosing the covariance of the spatial random effect remains the (spatial) support of the data. This practice is reasonable when the spatial data are generated from a process with unknown or nonexistent temporal dynamics. However, in many scientific systems it is likely that both the mean structure and observed pattern of spatial autocorrelation in the data are influenced by a known space-time generating process.

Consequently, the analysis of spatial data from processes with well-understood dynamics stands to benefit from more mechanistic modeling approaches, in which knowledge of the process dynamics implies a natural likelihood model for the data. Hanks (2017) suggests one approach for constructing mechanistic spa-

tial models: consider a science-based spatio-temporal process and find its stationary distribution. In particular, Hanks (2017) constructs a spatial model for genetic allele data by deriving the stationary distribution of an asymmetric random walk model for gene flow. The stationary distribution is a random field with discrete spatial support and a SAR covariance structure defined by the (parameterized) random walk model. The resulting mechanistic model was able to infer spatio-temporal movement rates from spatial data alone, providing important scientific insight that is unobtainable when using a standard semi-parametric random effect model. While this approach opens the door to building spatial models that directly result from spatio-temporal processes, the processes considered were limited. In particular, they were not allowed to have time varying noise; the spatial process was assumed to have reached a stationary distribution, at which it would continue constant in time.

We develop a set of mechanistic models for spatial data in which the underlying physical dynamics can be written as a linear SPDE with space-time varying Gaussian noise. In particular, the linear SPDE is approximated with a multivariate Ornstein-Uhlenbeck (OU) process defined over a discretized spatial domain, $\mathcal{S}$. This model is sufficiently flexible to accommodate space-time observations $\boldsymbol{Y_t} = (Y_1(t), \ldots, Y_n(t))'$ viewed as either a temporal snapshot of the transient or stationary distribution of the generative process. Furthermore, our model can be extended to spatial observations of the process averaged over a time interval $[0, T]$, defined as $\boldsymbol{V_T} = (V_1(T), \ldots, V_n(T))'$, where $V_i(T) = \frac{1}{T}\int_0^T Y_i(s)ds$. The latter includes observations of annual average sulfate concentrations, such as the SO_4 observations displayed in Figure 1(a).

In all cases, the underlying linear dynamics play a critical role in the construction of the spatial model's mean and covariance structure. These models are applicable to spatial data from a wide variety of applications, including many phenomena which can be approximated with a linear reaction-diffusion equation, such as point source pollution transport, invasive species dispersal, and population migration. Due to this general applicability, for the remainder of this section we present our methodology for the general class of linear space-time SPDEs defined by (3). When appropriate, we make explicit reference to the sulfate pollution system motivating these methods.

3.2. Approximating a Linear SPDE with an OU Process

In continuous space and time ($\boldsymbol{s} \in \mathcal{D}, t \geq 0$), let $y_{\boldsymbol{s}}(t)$ denote the process of interest, and consider the class of stochastic processes defined by

$$dy_{\boldsymbol{s}}(t) = \left(-\mathcal{A}_{\boldsymbol{s}}(\boldsymbol{\theta})y_{\boldsymbol{s}}(t) + m_{\boldsymbol{s}}(\boldsymbol{\theta})\right)dt + \xi_{\mathcal{B}}(\boldsymbol{s}, t), \tag{3}$$

where $\mathcal{A}_{\boldsymbol{s}}(\boldsymbol{\theta})$ denotes a linear differential operator (e.g., advection-diffusion), $m_{\boldsymbol{s}}(\boldsymbol{\theta})$ is a reaction term, and $\xi_{\mathcal{B}}(\boldsymbol{s}, t)$ is a space-time Gaussian noise process. The noise process is assumed to be white in time and spatially colored, with spatial covariance denoted by $\mathcal{B}$, which ensures that the process has a pointwise interpretation (Brown et al. 2000; Lindgren, Rue, and Lindström 2011; Sigrist, Künsch, and Stahel 2015; Bakka et al. 2020). Each component in (3) may be parameterized by a vector of process parameters, $\boldsymbol{\theta}$. For notational convenience, the explicit parameterization denoted by $\boldsymbol{\theta}$ is omitted in the remainder of this section. In addition, we assume that $\mathcal{A}_{\boldsymbol{s}}$ and $m_{\boldsymbol{s}}$ may vary in space, however, they are constant in time. Equation (3) encompasses a wide class of linear dynamical systems, including the mechanistic representation of sulfate transport described in Section 2.1.

Although the continuous-space formulation of (3) is appropriate from a scientific perspective, its distributional properties are challenging to understand. Consequently, it is convenient to consider a *discrete space approximation* to (3). Such an approximation can be constructed by first discretizing the continuous surface of interest, $\mathcal{D}$, into a finite collection of points, $\mathcal{S} = \{\boldsymbol{s}_1, \ldots, \boldsymbol{s}_n\}$, and then approximating the linear operator $\mathcal{A}$ with a matrix operator $\boldsymbol{A}$, which is defined with respect to $\mathcal{S}$. A variety of numerical schemes have been developed to facilitate these approximations, including finite difference (FDM), finite volume (FVM), and finite element methods (FEM), and the relative merits and implementation details of each method are often problem-specific (Versteeg and Malalasekera 2007; Johnson 2009). As a result, we focus our discussion on the distributional consequences of discretizing the space-time process defined in (3); additional discretization details, including an example discretization of an advection-diffusion process, can be found in the supplementary materials and the references therein.

By moving to discrete space, we can approximate the stochastic process in (3) with a multivariate Itô stochastic differential equation (SDE). Importantly, the stochastic process is now defined with respect to the discretization, $\mathcal{S}$, and $y_{\boldsymbol{s}}(t)$, $\mathcal{A}_{\boldsymbol{s}}$, $m_{\boldsymbol{s}}$, and $\xi_{\mathcal{B}}(\boldsymbol{s}, t)$ are replaced with their discrete counterparts. The continuous spatial surface, $y_{\boldsymbol{s}}(t)$, is restricted to an $n \times 1$ response vector $\boldsymbol{y}_t = (y_{1t}, \ldots, y_{nt})'$, where $y_{it} \equiv y_{\boldsymbol{s}_i}(t)$, $\boldsymbol{s}_i \in \mathcal{S}$. Similarly, the surface of sources/sinks, $m_{\boldsymbol{s}}$, is replaced with a vector, $\boldsymbol{m} = (m_{\boldsymbol{s}_1}, \ldots, m_{\boldsymbol{s}_n})'$, and the linear operator $\mathcal{A}_{\boldsymbol{s}}$ is replaced with its aforementioned sparse matrix approximation, $\boldsymbol{A}$. Finally, the space-time varying noise process, $\xi_{\mathcal{B}}(\boldsymbol{s}, t)$, is restricted to the discretized space, $\mathcal{S}$. Thus, we replace $\xi_{\mathcal{B}}(\boldsymbol{s}, t)$ with an $n \times 1$ vector of Gaussian noise, $\boldsymbol{B}d\boldsymbol{W}_t$ (i.e., $d\boldsymbol{W}_t$ is the distributional derivative of $\boldsymbol{W}_t$, where $\boldsymbol{W}_t = (W_1(t), \ldots, W_n(t))'$ is n-dimensional Brownian motion, with $W_i(t)$ corresponding to location $\boldsymbol{s}_i \in \mathcal{S}$, and $\boldsymbol{B}$ is the Cholesky decomposition of a spatial covariance matrix defined on $\mathcal{S}$). Substituting these discrete approximations into Equation (3) gives

$$d\boldsymbol{y}_t = \left(-\boldsymbol{A}\boldsymbol{y}_t + \boldsymbol{m}\right)dt + \boldsymbol{B}d\boldsymbol{W}_t. \tag{4}$$

We have approximated the continuous-space process (3) with a stochastic differential equation (SDE) (4) defined on a set of discrete spatial locations, $\mathcal{S}$; the process defined by this SDE is a multivariate Ornstein–Uhlenbeck (OU) process (Uhlenbeck and Ornstein 1930). The OU process has unique distributional properties—it is simultaneously Gaussian, Markov, and stationary (Doob 1942), and the process-dependent drift term in (4) results in a characteristic mean-reverting property. Consequently, we show that (4) can be used to define probabilistic models for spatial data observed from linear dynamical systems, as specified by (3).

3.3. Spatial Models for Snapshot Data

Assume that the initial state, $\boldsymbol{y}_0$, of the OU process $(\boldsymbol{y}_t)_{t\geq 0}$ in (4) is known. Then, for a nonsingular matrix $\boldsymbol{A}$, $(\boldsymbol{y}_t)_{t\geq 0}$ is a Gaussian process with solution at time t given by

$$\boldsymbol{y}_t = e^{-\boldsymbol{A}t}\boldsymbol{y}_0 + (\boldsymbol{I} - e^{-\boldsymbol{A}t})\boldsymbol{A}^{-1}\boldsymbol{m} + \int_0^t e^{-\boldsymbol{A}(t-s)}\boldsymbol{B}d\boldsymbol{W}_s, \quad (5)$$

where $e^{-\boldsymbol{A}t}$ denotes a matrix exponential and $\int_0^t e^{-\boldsymbol{A}(t-s)}\boldsymbol{B}d\boldsymbol{W}_s$ is a multivariate Itô integral (Øksendal 2003). Consequently, the *transient distribution* of the process at time t is

$$\boldsymbol{y}_t|\boldsymbol{y}_0 \sim N\left(e^{-\boldsymbol{A}t}\boldsymbol{y}_0 + (\boldsymbol{I} - e^{-\boldsymbol{A}t})\boldsymbol{A}^{-1}\boldsymbol{m}, \int_0^t e^{-\boldsymbol{A}(t-s)}\boldsymbol{B}\boldsymbol{B}'e^{-\boldsymbol{A}'(t-s)}ds\right). \quad (6)$$

This result follows directly from (5) (Gardiner 2004).

The transient distribution presented in (6) defines a spatial model for the spatio-temporal process assumed in (3). In particular, it assumes that the process was observed at some known time t, and that information about the initial state $\boldsymbol{y}_0$ is either known or desired. For example, during the outbreak of an invasive species (Hooten et al. 2007), the initial state represents the introduction of the agent into the system, and there may be known information about this introduction. By incorporating this information into (6), inference on the process dynamics—as defined by $\boldsymbol{A}$, $\boldsymbol{m}$, and $\boldsymbol{B}$—may be obtained from spatial data alone. In some cases inference about $\boldsymbol{y}_0$, such as the location or time the introduction most likely occurred, may itself be inferred from spatial data (Hefley et al. 2017).

However, in many systems little is known about the past, and directly characterizing $\boldsymbol{y}_0$ is difficult or impossible. For such scenarios, we instead consider the *stationary (time-limiting) distribution* of the OU process, which we denote as

$$\boldsymbol{y}_\infty = \lim_{t\to\infty} f(\boldsymbol{y}_t|\boldsymbol{y}_0), \quad (7)$$

where $f(\boldsymbol{y}_t|\boldsymbol{y}_0)$ is the transient distribution in (6). Assuming $\boldsymbol{A}$ has only eigenvalues with positive real part, the stationary distribution of (4) exists (Gardiner 2004) and is given as

$$\boldsymbol{y}_\infty \sim N\left(\boldsymbol{A}^{-1}\boldsymbol{m}, \boldsymbol{\Sigma}\right). \quad (8)$$

Here $\boldsymbol{\Sigma}$ is the solution to the continuous Lyapunov equation,

$$\boldsymbol{A}\boldsymbol{\Sigma} + \boldsymbol{\Sigma}\boldsymbol{A}' = \boldsymbol{B}\boldsymbol{B}'. \quad (9)$$

Solving the Lyapunov equation can quickly become computationally expensive as the size of $\boldsymbol{A}_{n\times n}$ increases. For example, the common Bartels–Stewart algorithm (Bartels and Stewart 1972) requires $\mathcal{O}(n^3)$ floating point operations, although for low-rank $\boldsymbol{B}$ faster methods are available (Simoncini 2007). In the case that $\boldsymbol{A} = \boldsymbol{A}'$ (i.e., $\boldsymbol{A}$ is symmetric) and $\boldsymbol{B} = \sigma\boldsymbol{I}$ (i.e., we assume the noise process has negligible spatial dependence on the discretized space, $\boldsymbol{S}$), the solution to (9) is simply $\boldsymbol{\Sigma} = \sigma^2\boldsymbol{A}^{-1}/2$, and the resulting stationary distribution of (4) is simply

$$\boldsymbol{y}_\infty \sim N\left(\boldsymbol{A}^{-1}\boldsymbol{m}, \frac{\sigma^2}{2}\boldsymbol{A}^{-1}\right). \quad (10)$$

Thus, in special cases the stationary distribution reduces to a spatial CAR model with precision $\frac{2}{\sigma^2}\boldsymbol{A}$.

Together, the transient and stationary distributions given in (6) and (8) form a class of mechanistic models for spatial data observed as a *snapshot* of a larger space-time process. In this "snapshot" observation, the time-scale of the space-time process should be much larger than the observational window in which the data were collected. For example, both daily sea surface temperatures and landscape genetics data might be considered realistic snapshots of their respective generating processes. In cases where additional information is known or desired about the initial state of the system, the data should be modeled using the transient distribution (6) of the OU process. When the initial state is unknown, or the process can reasonably be assumed to have reached stationarity, the data should be modeled using the stationary distribution (8).

3.4. Spatial Models for Time-Averaged Data

Spatial data are often collected and aggregated over a region of time. For example, the sulfate concentration depicted in Figure 1(a) is the concentration of SO_4^{2-} averaged over a year. The properties of the OU process allow us to extend our mechanistic spatial model to time-averaged spatial data. We show that the length of time over which spatial observations are aggregated has important implications on the second-order structure of the model.

Once again, consider the OU process defined by (4), and assume that $\boldsymbol{y}_0$ is a draw from the stationary distribution. Then $(\boldsymbol{y}_t)_{t\geq 0}$ is a Gaussian process with mean

$$\boldsymbol{\mu}(t) \equiv \boldsymbol{A}^{-1}\boldsymbol{m} \quad (11)$$

and covariance

$$k(s,t) \equiv Cov(\boldsymbol{y}_s, \boldsymbol{y}_t) = \begin{cases} \boldsymbol{\Sigma}e^{-\boldsymbol{A}'(t-s)}, & s < t \\ e^{-\boldsymbol{A}(s-t)}\boldsymbol{\Sigma} & t < s, \end{cases} \quad (12)$$

where $\boldsymbol{\Sigma}$ is the solution to the Lyapunov equation (9). If we then integrate this Gaussian process over a time window $[0, T]$ of length T, the resulting *time-averaged process* $(\boldsymbol{v}_T)_{T\geq 0}$ is also Gaussian, with

$$\boldsymbol{v}_T = \frac{1}{T}\int_0^T \boldsymbol{y}_s ds \sim N\left(\boldsymbol{A}^{-1}\boldsymbol{m}, \boldsymbol{\Psi}\right). \quad (13)$$

The covariance matrix, $\boldsymbol{\Psi}$, takes the form

$$\boldsymbol{\Psi} = \frac{1}{T}\left(\boldsymbol{A}'(\boldsymbol{B}\boldsymbol{B}')^{-1}\boldsymbol{A}\right)^{-1} - \frac{1}{T^2}\left[\boldsymbol{\Sigma}(\boldsymbol{I} - e^{-\boldsymbol{A}'T})(\boldsymbol{A}')^{-2} + \boldsymbol{A}^{-2}(\boldsymbol{I} - e^{-\boldsymbol{A}T})\boldsymbol{\Sigma}\right]. \quad (14)$$

This result is an extension of Doob's (1942) derivation of the distribution of displacements for a univariate OU process. Mathematical details are included in Appendix A.

The covariance $\boldsymbol{\Psi}$ of the time-averaged process can naturally be broken into two component parts,

$$\boldsymbol{\Phi} = \frac{1}{T}\left(\boldsymbol{A}'(\boldsymbol{B}\boldsymbol{B}')^{-1}\boldsymbol{A}\right)^{-1}, \quad (15)$$

and the remainder, $\boldsymbol{E} = \boldsymbol{\Psi} - \boldsymbol{\Phi}$. Notice that, from a computational perspective, $\boldsymbol{E}$ requires both the evaluation of a matrix exponential as well as the solution to the Lyapunov equation, two expensive tasks each of order $\mathcal{O}(n^3)$ flops. In contrast, the

operator matrix $\boldsymbol{A}$ is often sparse—a common property of most numerical approximation methods. If we again assume $\boldsymbol{B} = \sigma \boldsymbol{I}$, then $\boldsymbol{\Phi}$ now has the computationally convenient form

$$\boldsymbol{\Phi} = \frac{\sigma^2}{T}\left(\boldsymbol{A}'\boldsymbol{A}\right)^{-1}. \tag{16}$$

Thus, it is prudent to ask under what scenarios $\boldsymbol{\Phi}$ accurately approximates $\boldsymbol{\Psi}$ in (14).

For example, consider a homogeneous diffusion process with constant rate of decay, δ—a relatively simple model for the dispersal of air pollution about a source, or of species movement across a landscape. This process can be approximated by the linear operator $\boldsymbol{A} = (\gamma \boldsymbol{D} + \delta \boldsymbol{I})$, where $\boldsymbol{D}$ is a second-order central difference matrix and γ a constant rate of diffusion. For spatial data averaged over a given interval of time, $[0, T]$, how well does $\boldsymbol{\Phi}$ approximate the covariance matrix $\boldsymbol{\Psi}$ in (13)? In this case, we show (Appendix B) that

$$||\boldsymbol{E}||_2 = ||\boldsymbol{\Psi} - \boldsymbol{\Phi}||_2 \leq \frac{1}{T^2\delta^3}(1 - e^{-\delta T}). \tag{17}$$

For large δT, the remainder $\boldsymbol{E}$ goes to zero in the L_2 norm, and we have $\boldsymbol{\Psi} \approx \boldsymbol{\Phi}$. Thus, $\boldsymbol{\Phi}$ is an appropriate substitute for $\boldsymbol{\Psi}$ when either the observation length T or the rate of decay δ are large. More generally, $||\boldsymbol{E}||_2 \to 0$ as $T \to \infty$, and $\boldsymbol{\Psi}$ is well-approximated by $\boldsymbol{\Phi}$ for any aggregated space-time process in which T is sufficiently large to allow for repeated turnover of the system dynamics. In such scenarios, the approximated covariance $\boldsymbol{\Phi}$ (16) is in the form of a SAR model with precision matrix proportional to $\boldsymbol{A}'\boldsymbol{A}$.

3.5. Summary of OU Spatial Models

The proposed class of mechanistic spatial models are applicable to spatial data observed from a variety of dynamical systems. These models are especially useful for data observed from systems that are well-approximated by (locally) linear systems of equations, such as the reaction–advection–diffusion equation (potential applications include invasive species growth, population migration, pollution transport, cellular morphogenesis, etc.). After approximating these systems with a multivariate OU process, we obtain a familiar Gaussian process framework for modeling spatial data.

This approach has two main advantages over existing phenomenological spatial models. First, the underlying physical processes determine the spatial model's mean and covariance structure, implying that inference may be obtained on important components of the space-time dynamics from spatial data alone. This is especially useful for such systems where it is infeasible to observe spatial observations repeatedly in time. Second, the model is flexible enough to be used with three types of spatial data: observations made over a short temporal time frame (i.e., "snapshot" data) from either the process's transient or stationary distribution, and time-averaged spatial data assumed to be observed after the process has reached stationarity. As demonstrated, the temporal support of the spatial data has important consequences on the covariance structure of the model. In special cases, snapshot observations can be modeled with a Gaussian process with a CAR covariance structure with precision matrix proportional to the (sparse) matrix operator $\boldsymbol{A}$, while the covariance structure for time-averaged observations reduces to a SAR specification with precision proportional to $\boldsymbol{A}'\boldsymbol{A}$.

4. Analysis of Atmospheric Sulfate

We now apply this novel class of mechanistic spatial models to the 2011 annual sulfate data introduced in Section 2. To begin, we approximate the coupled, mechanistic representation of SO_4^{2-}–SO_2 in (1, 2) with an OU process (4) discretized on a 70×116 regular grid (cell area ~ 250 km^2). Letting $\boldsymbol{y}_t$ and $\boldsymbol{z}_t$ denote the vectorized $SO4^{2-}$ and SO_2 concentrations resulting from coal-fired power plant emissions, the discrete-space process is defined by

$$\boldsymbol{y}_t = \left[-(\gamma \boldsymbol{D} + \alpha \boldsymbol{C} + \delta \boldsymbol{I})\boldsymbol{y}_t + \eta \boldsymbol{z}_t\right] dt + \sigma\, d\boldsymbol{W}_t, \tag{18}$$

$$\boldsymbol{z}_t = \left[-(\gamma \boldsymbol{D} + \alpha \boldsymbol{C} + \eta \boldsymbol{I})\boldsymbol{z}_t + \beta \boldsymbol{X}\right] dt. \tag{19}$$

Here, $-(\gamma \boldsymbol{D} + \alpha \boldsymbol{C})$ is the finite volume method approximation of an advection-diffusion process caused by wind, where $\boldsymbol{D}$ is a second-order central difference matrix and $\boldsymbol{C}$ is a first-order upwind discretization, with edge flux assigned the interpolated 2011 average wind velocity (height = 10 m). See the supplementary materials for more discretization details, including a sensitivity analysis of the FVM grid size.

From a meteorological perspective, $\gamma \boldsymbol{D}$ represents transport due to sub-annual wind variability, while $\alpha \boldsymbol{C}$ denotes advection due to annual wind velocity. As before, δ is the rate of SO_4^{2-} deposition, while η is the rate at which SO_2 attributed to coal-fired power plants ($\boldsymbol{z_t}$) reacts into SO_4^{2-}. Thus, (18) corresponds to the SDE in (4), with $\boldsymbol{A} = (\gamma \boldsymbol{D} + \alpha \boldsymbol{C} + \delta \boldsymbol{I})$, $\boldsymbol{m}(t) = \eta \boldsymbol{z}_t$, and $\boldsymbol{B} = \sigma \boldsymbol{I}$. The coupled (deterministic) differential equation (19) explicitly links coal-fired power plant emissions of SO_2 ($\beta \boldsymbol{X}$) to the sulfate concentration, $\boldsymbol{y}_t$, through a similarly defined advection-diffusion process. Notably, the two processes (18, 19) are linked through the reaction of SO_2 emissions into SO_4^{2-} at rate η. An alternative model, driven by spatially correlated Brownian motion $\boldsymbol{B}d\boldsymbol{W}_t$, where $\boldsymbol{B}$ is the Cholesky decomposition of a Matérn covariance matrix defined on $\mathcal{S}$, was also considered. However, when assessed both qualitatively and with DIC, the model with negligible spatial dependence (i.e., $\boldsymbol{B} = \sigma \boldsymbol{I}$) was found to have a superior fit to the data

The 2011 observations used in our analysis are of *annual* average sulfate concentrations. Given the speed at which pollution transport occurs (Seinfeld and Pandis 2016), it is ill-advised to consider such data as a temporal snapshot. Instead, the time-averaged spatial model presented in Section 3.4 is an appropriate model for these data. Let $\boldsymbol{V}_T = \frac{1}{T}\int_0^T \boldsymbol{y}_t dt$ denote the averaged process over time T (in years). Similarly, let

$$\boldsymbol{Z}_{\boldsymbol{\theta},\boldsymbol{X}} \equiv \lim_{t\to\infty} \boldsymbol{z}_t = (\gamma \boldsymbol{D} + \alpha \boldsymbol{C} + \eta \boldsymbol{I})^{-1}(\beta \boldsymbol{X}) \tag{20}$$

denote the steady-state solution of the deterministic SO_2 process defined in (19), as determined by process parameters, $\boldsymbol{\theta}$, and the known SO_2 power plant emission levels, $\boldsymbol{X}$. Then, $\boldsymbol{V}_T$ may be appropriately modeled via the time-averaged mechanistic model (13),

$$\boldsymbol{V}_T \sim N\left(\boldsymbol{\mu}(\boldsymbol{\theta}, \boldsymbol{X}),\ \boldsymbol{\Sigma}_{\boldsymbol{\theta}}\right), \tag{21}$$

where

$$\boldsymbol{\mu}(\boldsymbol{\theta}, \boldsymbol{X}) = \boldsymbol{A}_{\boldsymbol{\theta}}^{-1}(\eta\, \boldsymbol{Z}_{\boldsymbol{\theta},\boldsymbol{X}}) \tag{22}$$

and

$$\boldsymbol{\Sigma}_{\boldsymbol{\theta}} = \frac{\sigma^2}{T}(\boldsymbol{A}_{\boldsymbol{\theta}}{}'\boldsymbol{A}_{\boldsymbol{\theta}})^{-1}. \tag{23}$$

This model is over-parameterized, as both γ and δ (components of $\boldsymbol{A}_{\boldsymbol{\theta}}$) control the spatial smoothness of the process. However, the rate of atmospheric deposition of SO_4^{2-} is quite fast (i.e., less than a week (Seinfeld and Pandis 2016)), and so we fix δ at 50. With a time scale of $T = 1$ year, this implies a rate of turnover consistent with the known process (Seinfeld and Pandis 2016). Thus, our mechanistic model for a complex space-time process—annual average SO_4^{2-} concentrations attributed to coal-fired power plant emissions of SO_2—has been reduced to a conveniently simple model, a familiar Gaussian process with mean $\boldsymbol{\mu}(\boldsymbol{\theta}, \boldsymbol{X})$ and SAR precision matrix $\boldsymbol{\Sigma}_{\boldsymbol{\theta}}^{-1}$ defined via the sparse matrix operator $\boldsymbol{A}_{\boldsymbol{\theta}}$ and the vector of SO_2 power plant emissions, $\boldsymbol{X}$.

4.1. Inference

We constructed a Markov chain Monte Carlo (MCMC) algorithm to sample from the posterior distribution of model parameters, given the observed 2011 SO_4^{2-} concentrations and coal-fired power plant emissions data. Updates for all model parameters except β were obtained using a random walk Metropolis step, with likelihood as defined in (21) and priors given in Table 1. For β, a full conditional Gibbs update was used. Five chains were run with randomly selected starting values, and each chain was run for 150,000 iterations, with the first 25,000 samples discarded as burn-in. Convergence was assessed qualitatively across the five chains.

Posterior mean estimates and 95% equal-tailed credible intervals are included in Table 1. Because (1) is a simple approximation to a complex process, not all parameter estimates have a clear scientific interpretation (e.g., β). However, some general trends can be inferred. The estimated rate of sub-annual wind transport, $\hat{\gamma} = 1535$, is much larger than the rate of advection due to annual average wind velocity, $\hat{\alpha} = 0.44$, implying that sub-annual variability in the wind field dominates observed SO_4^{2-} transport averaged over a year. Furthermore, the estimate $\hat{\eta} = 0.46$ implies that the SO_2 process acts as a smoothed source of SO_4^{2-}, centered about power plant locations. Finally, given the estimates of $\hat{\gamma}$ and $\hat{\alpha}$, $\hat{\sigma}^2 = 25{,}000$ implies that the marginal variances of the averaged SO_4^{2-} process (i.e., the marginal variances of $\hat{\boldsymbol{\Sigma}}_{\hat{\boldsymbol{\theta}}}$ from (21)) range from approximately 0.02 to 0.1.

Table 1. Parameter estimates for atmospheric SO_4^{2-} analysis.

Parameter	Interpretation	$\hat{\boldsymbol{\theta}} \approx \mathrm{E}(\boldsymbol{\theta}\,\vert\,\boldsymbol{Y})$	95% Credible interval	Prior
γ	Rate of sub-annual wind transport	1535	(1340, 1765)	Half-normal
α	Rate of annual wind transport	0.44	(0.01, 1.63)	Half-normal
η	$SO_2 \rightarrow SO_4^{2-}$	0.46	(0.32, 0.62)	Exponential
β	Proportional rate of SO_2 emission	4.18	(3.99, 4.48)	Half-normal
σ^2	B.M. process variance	25000	(19000, 32500)	Exponential
δ	Deposition of SO_4^{2-}	NA	NA	Fixed at 50

NOTE: Unit of time $T = 1$ year.

A qualitative comparison of the observed 2011 data with the estimated mean annual SO_4^{2-} concentrations attributed to SO_2 emissions (Figure 2), calculated as

$$\hat{\boldsymbol{V}} = \boldsymbol{A}_{\hat{\boldsymbol{\theta}}}^{-1}(\hat{\eta}\, \boldsymbol{Z}_{\hat{\boldsymbol{\theta}},\boldsymbol{X}}), \quad \hat{\boldsymbol{\theta}} = E(\boldsymbol{\theta}|\boldsymbol{V}), \tag{24}$$

provides additional insight regarding the inferred pollution dynamics. Recall that our dynamical system represents the annual average concentration of SO_4^{2-} ($\boldsymbol{V_T}$) due to SO_2 emissions from coal-fired power plants ($\boldsymbol{X}$). All other sources of SO_4 are assumed to be captured in the random noise process in (18). Thus, a comparison of the observed 2011 average sulfate concentrations against the estimated mean surface of sulfate pollution due to power plant emissions, $\hat{\boldsymbol{V}}$, can be used to both highlight geographic areas where observed SO_4^{2-} is likely due to power plant emissions, while at the same time identify areas in which observed SO_4^{2-} can most likely be attributed to alternative emissions sources.

For example, we see that the estimated mean SO_4^{2-} attributed to SO_2 power plant emissions (Figure 2(a)) is highest in the Ohio river valley, with a similar pocket of increased SO_4^{2-} in the Southeast. These estimated regions of high SO_4^{2-} exposure correspond to the locations of the largest SO_2 emitting power plants in the country (Figure 2(c)). Our model also identifies areas where the observed 2011 SO_4^{2-} concentrations are most likely due to sources other than power plant SO_2 emissions, particularly along the Mississippi River and the Gulf Coast. We hypothesize that the unexplained SO_4^{2-} in these areas is largely due to sulfur dioxide emissions from shipping traffic and heavy industrial activity (Mostert, Caris, and Limbourg 2017). Additional differences between the estimated and observed SO_4^{2-} concentrations can be attributed to random variation in SO_4^{2-} sources and sinks, which are included in the estimated covariance structure of our model.

For illustrative purposes, we compared the fitted model with three alternatives (see the supplementary materials for more details): (a) a time-averaged spatial model (13) with sulfur dioxide power plant emissions now included as a direct source of SO_4^{2-} (i.e., no coupling with SO_2; $\beta\boldsymbol{X}$ replaces $\eta\boldsymbol{Z}$ in (22)); (b) a stationary "snapshot" model (8) with the same coupled SO_2–SO_4 process as (18); and (c) a phenomenological spatial model, where the mean annual sulfate is modeled as the sum of weighted bivariate Gaussian functions centered at power plant locations, with the weight of each Gaussian function proportional to the facility's annual emissions total, and the covariance is modeled as a simultaneous autoregressive (SAR) process.

Model fit was assessed based on the deviance information criterion (DIC, Spiegelhalter et al. 2002), along with a qualitative assessment of posterior predictive draws from the process. The simplified process model (Alternative 1, DIC = −47,380), the snapshot model (Alternative 2, DIC = −43,140), and the phenomenological model (Alternative 3, DIC = −32,910) were found to be inferior to the time-averaged model with coupled SO_2–SO_4^{2-} (DIC = −47,790).

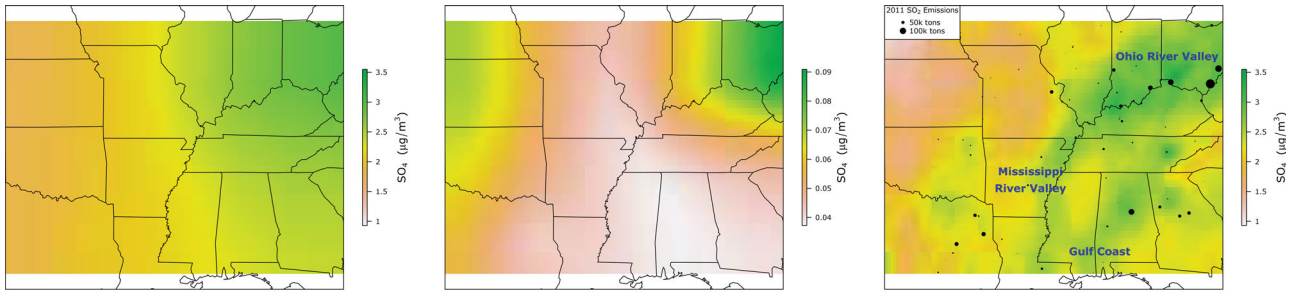

(a) Estimated mean SO_4. (b) Standard deviation. (c) Observed 2011 average SO_4.

Figure 2. A comparison of (a) the estimated mean SO_4^{2-} from power plant emissions and (b) the standard deviation of the estimated mean SO_4^{2-} with (c) the observed average 2011 sulfate concentrations.

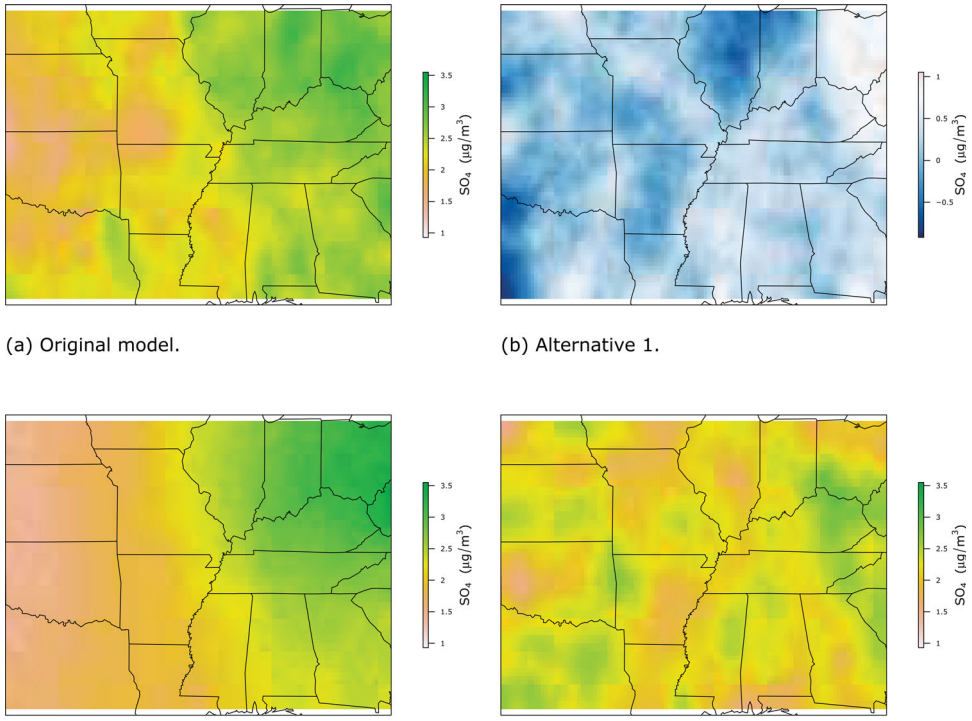

(a) Original model. (b) Alternative 1.

(c) Alternative 2. (d) Alternative 3.

Figure 3. Simulated realizations from the (a) time-averaged model with coupled SDE (the original model), (b) time-averaged model with uncoupled SDE (Alternative 1), (c) snapshot model with coupled SDE (Alternative 2), and (d) phenomenological model with SAR covariance (Alternative 3). Compared with the observed sulfate concentrations, the time-averaged SO_2–SO_4^{2-} model (a) performed best.

Similarly, a visual comparison of spatial fields sampled from the posterior distribution of each model (Figure 3) reveals the superiority of the time-averaged, coupled system. When compared with the observed 2011 sulfate concentrations (Figure 2(c)), the snapshot and phenomenological models (Alternatives 2 and 3) have misspecified error structures (Figures 3(b and d)), while the uncoupled process model (Alternative 1) has a problem with scale (Figure 3(b)). In contrast, the time-averaged model with joint SO_2–SO_4^{2-} matches the observed sulfate surface in both scale and spatial smoothness pattern (Figure 3(a)). These results indicate that (a) the temporal support of the data (in this case, annual sulfate concentrations) should be carefully considered when choosing an appropriate spatial model, and that (b) careful effort should be spent verifying that the key dynamics of the underlying scientific process are included in the OU process construction.

4.2. Estimating Human Exposure to SO_4^{2-}

An important advantage of mechanistic models for spatial data are their ability to provide probabilistic forecasts under alternative process scenarios. This is especially useful when assessing the regulatory impacts of power plant emissions on observed air pollution, which is a task traditionally left to deterministic physical–chemical models with limited ability to characterize uncertainty. For example, flue-gas desulfurization (FGD) technologies are used to remove (i.e., "scrub") SO_2 from coal-fired power plant emissions. Given the known impacts of SO_4^{2-} on human health (see Section 2), we estimate the population-weighted reduction in exposure to ambient sulfate attributable to FGD systems, and we consider which power plant facilities should be targeted with FGD systems in order to best reduce the overall human exposure to SO_4^{2-}.

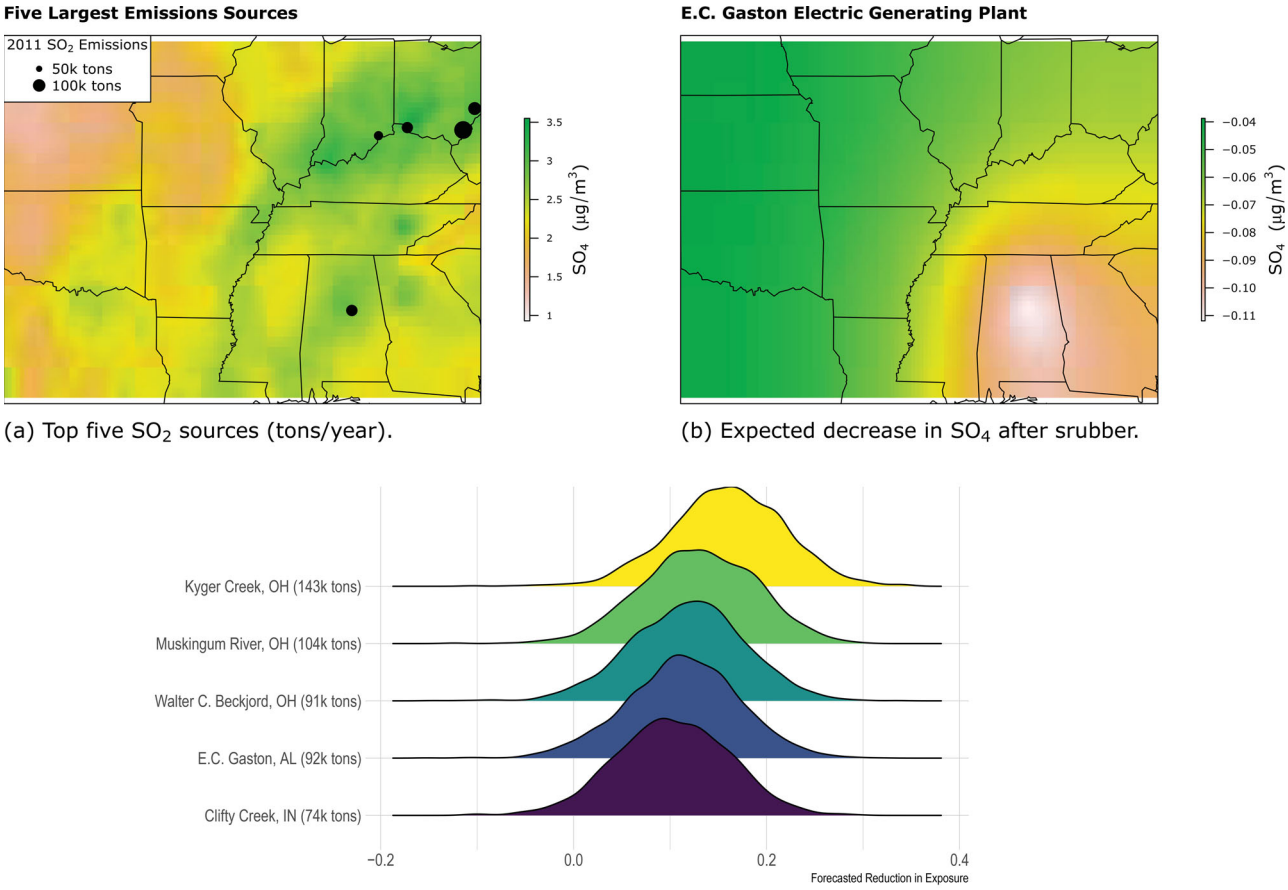

(a) Top five SO_2 sources (tons/year).

(b) Expected decrease in SO_4 after srubber.

(c) Probabilistic forecasts of the average reduction in human exposure to SO4 among five intervention scenarios; (·) denotes 2011 emissions totals (before FGD reduction).

Figure 4. A regulatory assessment of FGD scrubber intervention on annual SO_4^{2-} exposure among the top five SO_2 emitting facilities of 2011.

As an example, consider the five largest power plant facilities from our 2011 analysis (Figure 4(a)), based on the total amount of SO_2 emitted per facility. The inferred process dynamics from the fitted model (see (20) and (21)) can be used to create probabilistic estimates of the expected decrease in 2011 SO_4^{2-} concentration if an FGD scrubber had been in place at each facility. Let $\boldsymbol{X}_i^*$ denote the decrease in SO_2 emitted from facility i if an FGD scrubber had been in place in 2011. Using parameter samples from the posterior, $\boldsymbol{\theta}^{(k)} \sim \pi(\boldsymbol{\theta}|\boldsymbol{Y})$, we can simulate sample surfaces of the reduction in 2011 SO_4^{2-} after FGD scrubber implementation at facility i,

$$\hat{\boldsymbol{V}}_i^{(k)}|\boldsymbol{X}_i^* \sim N\left(\boldsymbol{\mu}(\boldsymbol{\theta}^{(k)}, \boldsymbol{X}_i^*), \boldsymbol{\Sigma}_{\theta^{(k)}}\right), \tag{25}$$

where $\boldsymbol{\mu}(\boldsymbol{\theta}^{(k)}, \boldsymbol{X}_i^*)$ and $\boldsymbol{\Sigma}_{\theta^{(k)}}$ are as defined in (21). For example, assuming a (conservative) 80% reduction in SO_2 emissions occurs after FGD scrubber implementation, Figure 4(b) shows the forecasted mean decrease in SO_4^{2-} attributed to the E.C. Gaston electric generating facility, calculated from 2000 simulated SO_4^{2-} surfaces as $\bar{\boldsymbol{V}}_i = \frac{1}{2000}\sum_{k=1}^{2000}\hat{\boldsymbol{V}}_i^{(k)}$.

The utility of these forecasts is especially useful when assessing regulatory interventions. Given possible resource limitations and the cost of installing FGD technologies, it is important to identify: (a) the reduction in human sulfate exposure attributable to existing FGD systems, and (b) the order in which untreated facilities should be targeted for FGD implementation. In 2011, FGD technologies were in place at 66 out of 193 power plants. Using draws from (25) and gridded 2010 U.S. population density data, we estimate that existing FGD technologies reduced 2011 population-weighted exposure to ambient sulfate by 1.97 $\mu g/m^3$ (95% credible interval (CI): 1.80–2.15). In addition, we estimate that installing FGD technologies at the five largest SO2-emitting facilities (Figure 4(c)) would reduce human exposure to ambient sulfate by an additional 0.45 $\mu g/m^3$ (95% CI: 0.33–0.54). Figure 4(c) suggests that adding scrubbers to the Kyger Creek facility should be a regulatory priority, as it results in the largest reduction in human exposure to SO_4^{2-} within the considered spatial domain, followed by the next four largest SO_2 facilities. However, despite emitting approximately *twice* as much SO_2 as Clifty Creek, its mean forecasted reduction in exposure due to FGD installation is about *1.5 times larger* than at Clifty Creek. Thus, intervention at Clifty Creek may have a larger epidemiological footprint than its emissions total would initially indicate. We are happy to report that, of the facilities still in operation in 2020 (Clifty Creek, E.C. Gaston, and Kyger Creek), all three have FGD technologies in place to reduce SO_2 emissions (U.S. EPA 2016).

5. Discussion

Models for spatial data are most often phenomenological, with a regression-based mean structure, and spatial autocorrelation modeled with a semiparametric random effect. This work proposes a new class of mechanistic models for spatial data that are constructed from OU processes. By first approximating the process with a discrete-space SDE, appropriate probability models can be constructed for spatial data viewed as (a) a temporal snapshot of the process, or (b) a time-averaged observation from the process. These models are versatile, and imply that inference on process parameters and probabilistic forecasts from transient and stationary space-time processes can be obtained from spatial data alone. As demonstrated in our analysis of 2011 SO_4^{2-} pollution and its relationship to sulfur dioxide emissions, these spatial models are especially useful for applications in which regulatory policy must be assessed.

It is important to compare the relative merits of our SO_4^{2-} pollution model against alternatives, including those more commonly found in atmospheric science. Our methodology is inspired by the rich history of mechanistic models for air pollution, including chemical transport models (Stein et al. 2015), plume models, and their so-called reduced-form hybrids (Foley et al. 2014; Heo, Adams, and Gao 2016). These models include detailed components for chemical transport, deposition, and reaction across three-dimensional space and across time, and are typically used to assess point-source pollution via the simulation of many individual-level trajectories (Henneman et al. 2019). This level of detail and model complexity is especially powerful when simulating air pollution concentrations and evaluating pollution sources on a small geographic or temporal extent. However, the large computational burden and lack of data-driven inference limits the utility of such models when assessing aggregate data over large spatial and temporal regions (Henneman et al. 2019). In contrast, our statistical model is directly tailored to SO_4^{2-} pollution aggregated over space and time, and we view its ability to infer (simplified) process dynamics and stochastic fluctuations on the time-scale of interest as its key advantage.

As shown in Section 4.2, one advantage of our mechanistic model over existing statistical models for spatial data is its ability to provide probabilistic forecasts and uncertainty quantification for systems with varying initial conditions. This is especially useful when modeling systems directly impacted by human intervention, such as air pollution resulting from coal-fired power plant emissions. Because of the known relationship between sulfate pollution and human health, one interesting application of this methodology is as a model of spatial treatment interference (see Zigler and Papadogeorgou 2021 and Karwa and Airoldi 2018). For example, a causal analysis of the effect of FGD scrubber implementation on county-level human health outcomes requires a mapping of the treatment at power plant facility i to all downwind population locations. Existing methodologies often seek to define such "exposure mappings" via static networks relating treatments to outcomes (Aronow and Samii 2017; Karwa and Airoldi 2018; Zigler, Forastiere, and Mealli 2020). However, given our knowledge of the physical system relating SO_2 emissions to SO_4^{2-} concentrations and our model's ability to infer these dynamics, our mechanistic model may be a preferred specification of treatment exposure. We plan to explore the utility of this model as an exposure mapping, assessing how uncertainty and the presence of environmental confounders may be incorporated into existing causal inference methodology in the presence of interference.

Finally, the connections between the continuous space SPDE and discrete space SDE introduced in Section 3.2 presents a path for future development of mechanistic spatial models. Broader classes of SDEs, including alternative mean-reverting processes and models driven by Lévy processes besides Brownian motion, may result in probability models for spatial data from a much broader class of space-time systems. In particular, a stationary process that allows for periodic fluctuations in the mean would allow for a larger class of mechanisms to be modeled, including the addition of seasonal wind patterns in our model of atmospheric sulfate. Although we view discretization as an essential computational procedure for these mechanistic spatial models, additional connections between the implied spatial models constructed from the OU process and continuous space-time processes such as those presented by Brown et al. (2000), Brix and Diggle (2001), Sigrist, Künsch, and Stahel (2015) and Bakka et al. (2020) may prove fruitful in improving our understanding of the appropriateness of certain families of covariance functions for spatial data.

Appendix A: Derivation of the Time-Averaged OU Process

The result follows from the well-known property (Doob 1942) that the integral of a Gaussian process $(Y_t)_{t\geq 0}$ with mean $\mu(t)$ and covariance $k(s,t)$ is itself a Gaussian process, where $V_T = \int_0^T Y_s ds$ has mean

$$\mathrm{E}(V_T) = \int_0^T \mu(s) ds \tag{A.1}$$

and variance

$$\mathrm{var}(V_T) = \int_0^T \int_0^T k(s,t) ds dt. \tag{A.2}$$

Thus, for the space-time OU process defined by (4), with $\boldsymbol{\mu}(t)$ and $k(s,t)$ given in (11) and (12), we have

$$\int_0^T \boldsymbol{\mu}(s) ds = \int_0^T \boldsymbol{A}^{-1}\boldsymbol{m} ds = T\boldsymbol{A}^{-1}\boldsymbol{m}, \tag{A.3}$$

and

$$\begin{aligned}
&\int_0^T \int_0^T k(s,t) ds dt \\
&= \int_0^T \left(\int_0^t \boldsymbol{\Sigma} e^{-\boldsymbol{A}'(t-s)} ds + \int_t^T e^{-\boldsymbol{A}(s-t)} \boldsymbol{\Sigma} ds \right) dt && \text{(A.4)} \\
&= \int_0^T \left(\boldsymbol{\Sigma}(\boldsymbol{I} - e^{-\boldsymbol{A}'t})(\boldsymbol{A}')^{-1} + \boldsymbol{A}^{-1}(\boldsymbol{I} - e^{-\boldsymbol{A}(T-t)})\boldsymbol{\Sigma} \right) dt && \text{(A.5)} \\
&= T\left(\boldsymbol{\Sigma}(\boldsymbol{A}')^{-1} + \boldsymbol{A}^{-1}\boldsymbol{\Sigma} \right) - \boldsymbol{\Sigma}(\boldsymbol{I} - e^{-\boldsymbol{A}'T})(\boldsymbol{A}')^{-2} \\
&\quad - \boldsymbol{A}^{-2}(\boldsymbol{I} - e^{-\boldsymbol{A}T})\boldsymbol{\Sigma}. && \text{(A.6)}
\end{aligned}$$

Finally, from the Lyapunov equation (9) we see that

$$\left(\boldsymbol{\Sigma}(\boldsymbol{A}')^{-1} + \boldsymbol{A}^{-1}\boldsymbol{\Sigma} \right) = \left(\boldsymbol{A}'(\boldsymbol{B}\boldsymbol{B}')^{-1}\boldsymbol{A} \right)^{-1} \tag{A.7}$$

and the result follows.

Appendix B: An Error Bound for the Time-Averaged Covariance

Let $\boldsymbol{A} = (\gamma \boldsymbol{D} + \delta \boldsymbol{I})$ be an FDM or FVM approximation to a homogeneous diffusion process (rate of diffusion γ) with rate of decay δ. Then $\boldsymbol{A}$ is symmetric, and

$$\boldsymbol{E} = \boldsymbol{\Psi} - \boldsymbol{\Phi} = \frac{-1}{T^2}(\boldsymbol{I} - e^{-\boldsymbol{A}T})\boldsymbol{A}^{-3}. \tag{B.1}$$

Under either periodic or zero flux boundary conditions, the diffusion operator matrix, $\boldsymbol{D}_{n\times n}$, is (a) symmetric with real elements, and (b) weakly diagonally dominant. Thus, by the Gershgorin circle theorem, the eigenvalues λ_i are all real and nonnegative, with $\lambda_{(n)} = \min_i \lambda_i = 0$. Let $\boldsymbol{\Lambda}$ be a diagonal matrix with $\boldsymbol{\Lambda}_{ii} = \lambda_i$. Factorizing $\boldsymbol{D}$ into its canonical form gives $\boldsymbol{D} = \boldsymbol{U}\boldsymbol{\Lambda}\boldsymbol{U}'$, where $\boldsymbol{U}$ is the square $n \times n$ matrix whose ith column is the eigenvector u_i of $\boldsymbol{D}$. Thus, $\boldsymbol{A}$ can be factorized as

$$\boldsymbol{A} = \gamma \boldsymbol{D} + \delta \boldsymbol{I} = \boldsymbol{U}\boldsymbol{V}\boldsymbol{U}', \tag{B.2}$$

where $\boldsymbol{V}$ is a diagonal matrix with $v_i \equiv V_{ii} = \gamma\lambda_i + \delta$. Note that $v_{(n)} = \gamma\lambda_{(n)} + \delta = \delta$. Then,

$$||\boldsymbol{E}||_2 = ||\frac{1}{T^2}(\boldsymbol{I} - e^{-\boldsymbol{A}T})\boldsymbol{A}^{-3}||_2 \tag{B.3}$$

$$= ||\frac{1}{T^2}\boldsymbol{U}(\boldsymbol{I} - e^{-\boldsymbol{V}T})\boldsymbol{V}^{-3}\boldsymbol{U}'||_2 \tag{B.4}$$

$$\leq ||\boldsymbol{U}||_2||\boldsymbol{U}'||_2||\frac{1}{T^2}(\boldsymbol{I} - e^{-\boldsymbol{V}T})\boldsymbol{V}^{-3}||_2 \tag{B.5}$$

$$= ||\frac{1}{T^2}(\boldsymbol{I} - e^{-\boldsymbol{V}T})\boldsymbol{V}^{-3}||_2 \tag{B.6}$$

$$= \frac{1}{T^2\delta^3}(1 - e^{-\delta T}). \tag{B.7}$$

The final equality uses the fact that $\frac{1}{T^2}(\boldsymbol{I} - e^{-\boldsymbol{V}T})\boldsymbol{V}^{-3}$ is a diagonal matrix with ith diagonal, $(1-e^{-v_iT})/(T^2v_i^3)$. This function is decreasing in v_i. Thus, $||\frac{1}{T^2}(\boldsymbol{I} - e^{-\boldsymbol{V}T})\boldsymbol{V}^{-3}||_2 = \frac{1}{T^2\delta^3}(1 - e^{-\delta T})$.

Supplementary Materials

The supplementary materials include a sensitivity analysis of the discretization grid size, details on the numerical approximation of the differential operator, and a description of the three alternative models discussed in Section 4.1, as well as R code which replicates the results of this analysis.

Acknowledgments

We thank the editor and two anonymous reviewers for their helpful comments.

Funding

This work was partially supported by research funding from NSF DMS-2015273, NIH R01ES026217, and EPA 83587201. This publication's contents are solely the responsibility of the grantee and do not necessarily represent the official views of the Environmental Protection Agency. Further, the Environmental Protection Agency does not endorse the purchase of any commercial products or services mentioned in this publication.

References

Aas, W., Mortier, A., Bowersox, V., Cherian, R., Faluvegi, G., Fagerli, H., Hand, J., Klimont, Z., Galy-Lacaux, C., Lehmann, C. M. B., Myhre, C. L., Myhre, G., Olivié, D., Sato, K., Quaas, J., Rao, P. S. P., Schulz, M., Shindell, D., Skeie, R. B., Stein, A., Takemura, T., Tsyro, S., Vet, R., and Xu, X. (2019), "Global and Regional Trends of Atmospheric Sulfur," *Scientific Reports*, 9, 953. [1]

Aronow, P. M., and Samii, C. (2017), "Estimating Average Causal Effects Under General Interference, with Application to a Social Network Experiment," *The Annals of Applied Statistics*, 11, 1912–1947. [10]

Bai, L., Shin, S., Kwong, J., Hystad, P., van Donkelaar, A., Goldberg, M., Lavigne, E., Weichenthal, S., Martin, R. V., Copes, R., Kopp, A., and Chen, H. (2019a), "Exposure to Ambient Air Pollution and the Incidence of Lung Cancer and Breast Cancer in the Ontario Population Health and Environment Cohort," *International Journal of Cancer*, 146, 2450–2459. [1]

Bai, L., Shin, S., Burnett, R. T., Kwong, J. C., Hystad, P., van Donkelaar, A., Goldberg, M. S., Lavigne, E., Copes, R., Martin, R. V., Kopp, A., and Chen, H. (2019b), "Exposure to Ambient Air Pollution and the Incidence of Congestive Heart Failure and Acute Myocardial Infarction: A Population-Based Study of 5.1 Million Canadian Adults Living in Ontario," *Environment International*, 132, 105004. [1]

Bakka, H., Krainski, E., Bolin, D., Rue, H., and Lindgren, F. (2020), "The Diffusion-Based Extension of the Matérn Field to Space-Time." arXiv:2006.04917. [4,10]

Banerjee, S., Carlin, B. P., and Gelfand, A. E. (2004), *Hierarchical Modeling and Analysis for Spatial Data*, Boca Raton, FL: Chapman & Hall/CRC Press LLC. [3]

Bartels, R. H., and Stewart, G. W. (1972), "Solution of the Matrix Equation ax + xb = c," *Communications of the ACM*, 15, 820–826. [5]

Besag, J. (1974), "Spatial Interaction and the Statistical Analysis of Lattice Systems," *Journal of the Royal Statistical Society*, Series B, 36, 192–236. [3]

Brix, A., and Diggle, P. J. (2001), "Spatiotemporal Prediction for Log-Gaussian Cox Processes," *Journal of the Royal Statistical Society*, Series B, 63, 823–841. [10]

Brook, R. D., Rajagopalan, S., Pope, C. A., Brook, J. R., Bhatnagar, A., Diez-Roux, A. V., Holguin, F., Hong, Y., Luepker, R. V., Mittleman, M. A., Peters, A., Siscovick, D., SmithJr, S. C., Whitsel, L., Kaufman J. D., and American Heart Association Council on Epidemiology and Prevention, Council on the Kidney in Cardiovascular Disease, and Council on Nutrition, Physical Activity and Metabolism (2010), "Particulate Matter Air Pollution and Cardiovascular Disease," *Circulation*, 121, 2331–2378. [2]

Brown, P. E., Karesen, K. F., Roberts, G. O., Tonellato, S. (2000), "Blur-Generated Non-separable Space-Time Models," *Journal of the Royal Statistical Society*, Series B, 62, 847–860. [4,10]

Cressie, N. (1993), *Statistics for Spatial Data*, New York: Wiley. [3]

Cressie, N., and Wikle, C. K. (2011), *Statistics for Spatio-Temporal Data*, New York: Wiley. [3]

Dominici, F., Greenstone, M., and Sunstein, C. R. (2014), "Particulate Matter Matters," *Science*, 344, 257–259. [1,2]

Doob, J. L. (1942), "The Brownian Movement and Stochastic Equations," *Annals of Mathematics*, 43, 351–369. [4,10]

Foley, K. M., Napelenok, S. L., Jang, C., Phillips, S., Hubbell, B. J., Fulcher, C. M. (2014), "Two Reduced Form Air Quality Modeling Techniques for Rapidly Calculating Pollutant Mitigation Potential Across Many Sources, Locations and Precursor Emission Types," *Atmospheric Environment*, 98, 283–289. [1,10]

Gardiner, C. W. (2004), "*Handbook of Stochastic Methods* (3rd ed.), Berlin: Springer-Verlag. [5]

Guan, Y., Johnson, M. C., Katzfuss, M., Mannshardt, E., Messier, K. P., Reich, B. J., Song, J. J. (2020), "Fine-Scale Spatiotemporal Air Pollution Analysis Using Mobile Monitors on Google Street View Vehicles," *Journal of the American Statistical Association*, 115, 1111–1124. [1]

Hanks, E. M. (2017), "Modeling Spatial Covariance Using the Limiting Distribution of Spatio-Temporal Random Walks," *Journal of the American Statistical Association*, 112, 497–507. [3,4]

Hefley, T. J., Hooten, M. B., Hanks, E. M., Russell, R. E., and Walsh, D. P. (2017), "Dynamic Spatio-Temporal Models for Spatial Data," *Spatial Statistics*, 20, 206–220. [5]

Hefley, T. J., Hooten, M. B., Russell, R. E., Walsh, D. P., and Powell, J. A., (2017), "When Mechanism Matters: Bayesian Forecasting Using Models of Ecological Diffusion," *Ecology Letters*, 20, 640–650. [3]

Henneman, L. R., Choirat, C., Ivey, C., Cummiskey, K., and Zigler, C. M., (2019), "Characterizing Population Exposure to Coal Emissions Sources

in the United States Using the Hyads Model," *Atmospheric Environment*, 203, 271–280. [2,10]

Heo, J., Adams, P. J., and Gao, H. O. (2016), "Reduced-Form Modeling of Public Health Impacts of Inorganic pm2.5 and Precursor Emissions," *Atmospheric Environment*, 137, 80–89. [1,10]

Hooten, M. B., Wikle, C. K., Dorazio, R. M., and Royle, J. A. (2007), "Hierarchical Spatiotemporal Matrix Models for Characterizing Invasions," *Biometrics*, 63, 558–567. [5]

Johnson, C. (2009), *Numerical Solution of Partial Differential Equations by the Finite Element Method*, New York: Dover Publications Inc. [4]

Kalnay, E., Kanamitsu, M., Kistler, R., Collins, W., Deaven, D., Gandin, L., Iredell, M., Saha, S., White, G., Woollen, J., Zhu, Y., Chelliah, M., Ebisuzaki, W., Higgins, W., Janowiak, J., Mo, K. C., Ropelewski, C., Wang, J., Leetmaa, A., Reynolds, R., Jenne, R., and Joseph, D. (1996), "The NCEP/NCAR 40-year Reanalysis Project," *Bulletin of the American Meteorological Society*, 77, 437–470. [2]

Karwa, V., and Airoldi, E. M. (2018), "A Systematic Investigation of Classical Causal Inference Strategies Under Mis-specification Due to Network Interference." arXiv:1810.08259. [10]

Kaufmann, R. K., Kauppi, H., Mann, M. L., and Stock, J. H. (2011), "Reconciling Anthropogenic Climate Change with Observed Temperature 1998-2008," *Proceedings of the National Academy of Sciences of the United States of America*, 108, 11790–11793. [1]

Lindgren, F., Rue, H., and Lindström, J. (2011), "An Explicit Link Between Gaussian Fields and Gaussian Markov Random Fields: The Stochastic Partial Differential Equation Approach," *Journal of the Royal Statistical Society*, Series B, 73, 423–498. [3,4]

Massetti, E., Brown, M. A., Lapsa, M. V., Sharma, I., Bradbury, J., Cunliff, C., and Li, Y. (2017), "Environmental Quality and the U.S. Power Sector: Air Quality, Land Use and Environmental Justice." Technical report from the U.S. Department of Energy, Oak Ridge National Lab, Research Org.: ORNL Sponsoring Org. USDOE OSTI Identifier: 1339359 Report Number: ORNL/SPR-2016/772. doi: 10.2172/1339359. [3]

Mostert, M., Caris, A., and Limbourg, S. (2017), "Road and Intermodal Transport Performance: The Impact of Operational Costs and Air Pollution External Costs," *Research in Transportation Business and Management*, 23, 75–85. [7]

Ng, C. F. S., Hashizume, M., Obase, Y., Doi, M., Tamura, K., Tomari, S., Kawano, T., Fukushima, C., Matsuse, H., Chung, Y., Kim, Y., Kunimitsu, K., Kohno, S., and Mukae, H. (2019), "Associations of Chemical Composition and Sources of pm2.5 with Lung Function of Severe Asthmatic Adults in a Low Air Pollution Environment of Urban Nagasaki, Japan," *Environmental Pollution*, 252, 599–606. [1]

Øksendal, B. (2003), *Stochastic Differential Equations: An Introduction with Applications* (6th ed.), Berlin: Springer-Verlag. [5]

Rowe, M. D. (1980), "Human Exposure to Sulfates from Coal-Fired Power Plants," *Journal of the Air Pollution Control Association*, 30, 682–684. [1]

Seinfeld, J. H., and Pandis, S. N. (2016), *Atmospheric Chemistry and Physics: From Air Pollution to Climate Change* (3rd ed.), Hoboken, NJ: Wiley. [3,6,7]

Sigrist, F., Künsch, H. R., Stahel, W. A. (2015), "Stochastic Partial Differential Equation Based Modelling of Large Space–Time Data Sets," *Journal of the Royal Statistical Society*, Series B, 77, 3–33. [4,10]

Simoncini, V. (2007), "A New Iterative Method for Solving Large-Scale Lyapunov Matrix Equations," *SIAM Journal on Scientific Computing*, 29, 1268–1288. [5]

Spiegelhalter, D. J., Best, N. G., Carlin, B. P., and Van Der Linde, A. (2002), "Bayesian Measures of Model Complexity and Fit," *Journal of the Royal Statistical Society*, Series B, 64, 583–639. [7]

Stein, A. F., Draxler, R. R., Rolph, G. D., Stunder, B. J. B., Cohen, M. D., and Ngan, F. (2015), "Noaa's Hysplit Atmospheric Transport and Dispersion Modeling System," *Bulletin of the American Meteorological Society*, 96, 2059–2077. [1,10]

Tessum, C. W., Hill, J. D., and Marshall, J. D. (2017), "Inmap: A Model for Air Pollution Interventions," *PLOS ONE*, 12, 1–26. [3]

Uhlenbeck, G. E., and Ornstein, L. S. (1930), "On the Theory of the Brownian Motion," *Physical Review*, 36, 823–841. [4]

U.S. EPA. (2003), "Latest Findings on National Air Quality: 2002 Status and Trends." Available at *https://www.epa.gov/air-trends/historical-air-quality-trends-reports*. [1]

——— (2016), "Air Markets Program Data." Available at *https://ampd.epa.gov/ampd/*. [2,9]

van Donkelaar, A., Martin, R. V., Li, C., and Burnett, R. T. (2019), "Regional Estimates of Chemical Composition of Fine Particulate Matter Using a Combined Geoscience-Statistical Method with Information from Satellites, Models, and Monitors," *Environmental Science & Technology*, 53, 2595–2611. [1,2]

Ver Hoef, J. M., Hanks, E. M., and Hooten, M. B. (2018), "On the Relationship Between Conditional (car) and Simultaneous (sar) Autoregressive Models," *Spatial Statistics*, 25, 68–85. [3]

Versteeg, H. K., and Malalasekera, W. (2007), *An Introduction to Computational Fluid Dynamics: The Finite Volume Method* (2nd ed.), Harlow, UK: Pearson Education Ltd. [4]

Ward, P. L. (2009), "Sulfur Dioxide Initiates Global Climate Change in Four Ways," *Thin Solid Films*, 517, 3188–3203. [1]

Whittle, P. (1954), "On Stationary Processes in the Plane," *Biometrika*, 44, 434–449. [3]

——— (1962), "Topographic Correlation, Power-Law Covariance Functions, and Diffusion," *Biometrika*, 49, 305–314. [3]

Wikle, C. K., and Hooten, M. B. (2010), "A General Science-Based Framework for Dynamical Spatio-Temporal Models," *TEST*, 19, 417–451. [3]

Zigler, C., Forastiere, L., and Mealli, F. (2020), "Bipartite Interference and Air Pollution Transport: Estimating Health Effects of Power Plant Interventions." arXiv:2012.04831. [1,2,10]

Zigler, C. M., and Papadogeorgou, G. (2021), "Bipartite Causal Inference with Interference," *Statistical Science*, 36, 109–123. [1,10]